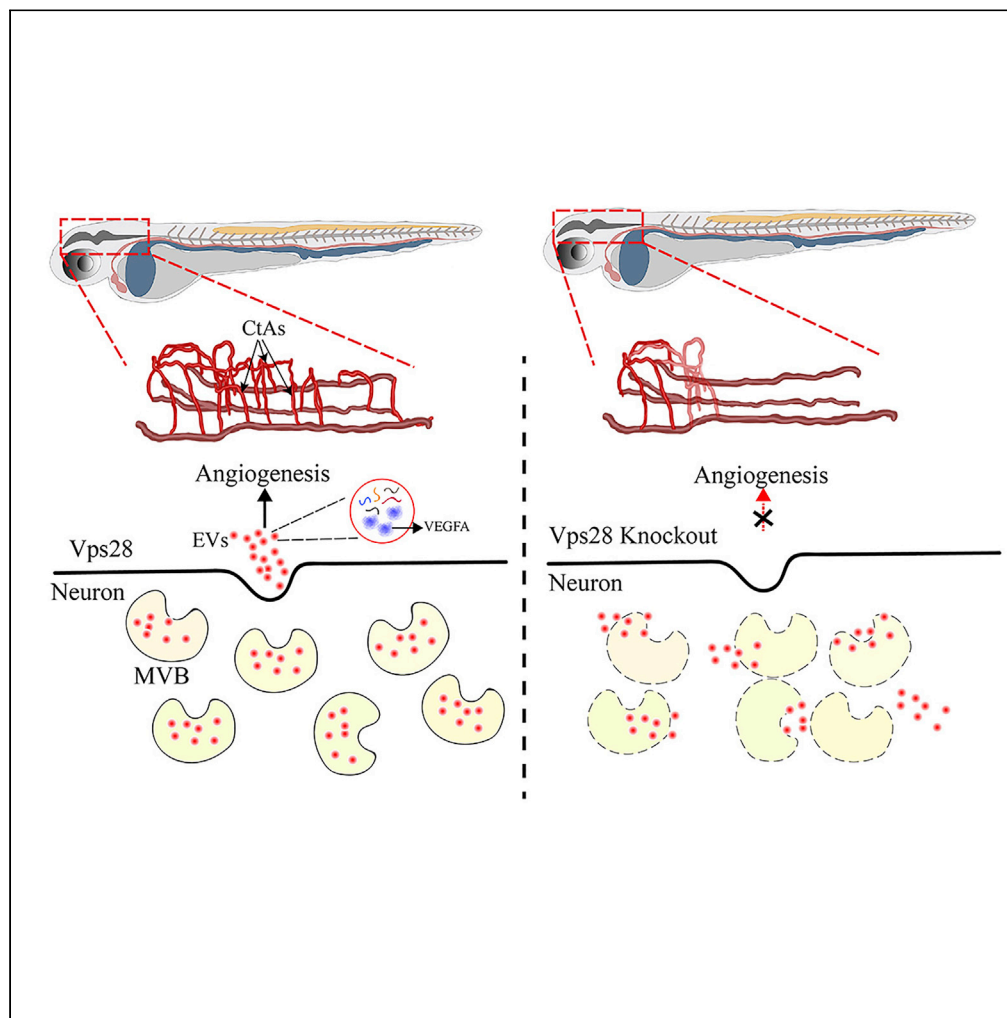


Article

# VPS28 regulates brain vasculature by controlling neuronal VEGF trafficking through extracellular vesicle secretion



Xiaohua Dong,  
Dongya Jiang,  
Long Wang, ...,  
Qingshun Zhao,  
Guangming  
Zhang, Xinyuan Li

njfishxiaohua@163.com (X.D.)  
yingmin\_hosp@126.com (Y.Z.)  
qingshun@nju.edu.cn (Q.Z.)  
gmzhangyj@163.com (G.Z.)  
lxy2186@shtrhospital.com  
(X.L.)

Highlights

Vps28 is highly expressed in neurons and involved in the secretion of neuronal EVs

Vps28, as a subunit of ESCRT-1 complexes, participates in the formation of MVB

Vps28 plays an important role in VEGFA transport and promotes neurovascular communication

Dong et al., iScience 25,  
104042  
April 15, 2022 © 2022 The  
Author(s).  
[https://doi.org/10.1016/  
j.isci.2022.104042](https://doi.org/10.1016/j.isci.2022.104042)



## Article

## VPS28 regulates brain vasculature by controlling neuronal VEGF trafficking through extracellular vesicle secretion

Xiaohua Dong,<sup>1,2,3,6,7,\*</sup> Dongya Jiang,<sup>4,6</sup> Long Wang,<sup>5,6</sup> Jing Zhao,<sup>1</sup> Lingling Yu,<sup>3</sup> Yun Huang,<sup>3</sup> Xiaohui Wu,<sup>3</sup> Yanqing Zhu,<sup>3</sup> Yingmin Zhao,<sup>3,\*</sup> Qingshun Zhao,<sup>4,\*</sup> Guangming Zhang,<sup>2,\*</sup> and Xinyuan Li<sup>1,\*</sup>

## SUMMARY

**Extracellular vesicles (EVs) participate in intercellular communication and contribute to the angiogenesis. However, the understanding of the mechanisms underlying EVs secretion by neurons and their action on the vascular system of the central nervous system (CNS) remain rudimentary. Here, we show that vacuolar protein sorting 28 (Vps28) is essential for the sprouting of brain central arteries (CtAs) and for the integrity of blood-brain barrier (BBB) in zebrafish. Disruption of neuron-enriched Vps28 significantly decreased EVs secretion by regulating the formation of intracellular multivesicular bodies (MVBs). EVs derived from zebrafish embryos or mouse cortical neurons partially rescued the brain vasculature defect and brain leakage. Further investigations revealed that neuronal EVs containing vascular endothelial growth factor A (VEGF-A) are key regulators in neurovascular communication. Our results indicate that Vps28 acts as an intercellular endosomal regulator mediating the secretion of neuronal EVs, which in turn communicate with endothelial cells to mediate angiogenesis through VEGF-A trafficking.**

## INTRODUCTION

The formation and connection of a functional vasculature is essential for embryogenesis and plays a crucial role in tissue and organ homeostasis. The development of cranial vasculature in zebrafish follows a stereotypical growth pattern with regard to vasculogenesis and angiogenesis (Isogai et al., 2001). Cerebral vascularization is critical because the interaction of the vasculature with the CNS forms the BBB, which is essential in maintaining a self-balancing environment for proper functioning of the brain (Daneman and Prat, 2015; Langen et al., 2019; Obermeier et al., 2013). The basilar artery (BA), primordial hindbrain channels (PHBCs), and the central arteries (CtAs) constitute the main vascular network of the CNS during the embryogenesis in zebrafish (Isogai et al., 2001; Ulrich et al., 2011). CtAs constitute an important network of vessels penetrating through the hindbrain and are necessary for the correct connection between the PHBCs and the BA (Gore et al., 2012; Ulrich et al., 2011).

CNS vascularization is controlled and organized by multiple neural-derived classical angiogenic factors, such as vascular endothelial growth factor (VEGF) and Wnt7a/b, through neurovascular communication (Paredes et al., 2018). Neural tube-derived VEGF-A is essential for the formation of the perineural vascular plexus and induction of ectopic ingression of blood vessels into the CNS parenchyma (Himmels et al., 2017; James et al., 2009). In radial glia-ablated zebrafish with reduced Vegfab expression within the spinal cord, the vertebral arteries were reported to be completely absent (Matsuoka et al., 2017). VEGF is evolutionarily conserved among vertebrate species. VEGF and sFlt1 expressed by motor neurons are required for blood vessel patterning around the motor neuron columns of the developing spinal cord in mouse and chick embryos (Himmels et al., 2017). Astrocyte-derived VEGF guides the retinal angiogenesis in the early stages of life in newborn mice (Gerhardt et al., 2003). Recently, microRNAs have been described as an additional factor essential for development of endothelial cells (ECs) during CNS angiogenesis and establishment of BBB integrity (Madelaine et al., 2017; Xu et al., 2017). Although numerous research studies have reported that neural-derived signals control CNS angiogenesis, the mechanism underlying the communication for transport of these neural signals and support for survival and sprouting of ECs is not fully understood.

<sup>1</sup>Department of Neurosurgery, Tongren Hospital, Shanghai Jiao Tong University School of Medicine, 1111 XianXia Road, Shanghai 20033, China

<sup>2</sup>Department of Anesthesiology, Tongren Hospital, Shanghai Jiao Tong University School of Medicine, 1111 XianXia Road, Shanghai 20033, China

<sup>3</sup>Department of Pediatric, Jingjiang People's Hospital Affiliated to Yangzhou University, Jingjiang 214500, China

<sup>4</sup>Ministry of Education Key Laboratory of Model Animal for Disease Study, Model Animal Research Center, Nanjing University, Nanjing 210061, China

<sup>5</sup>Department of Cardiology, Key Laboratory of Clinical Cancer Pharmacology and Toxicology Research of Zhejiang Province, the Affiliated Hangzhou First People's Hospital of Zhejiang University School of Medicine, Hangzhou, Zhejiang, China

<sup>6</sup>These authors contributed equally

<sup>7</sup>Lead contact

\*Correspondence:

[nfshxiaohua@163.com](mailto:nfshxiaohua@163.com) (X.D.),

[yingmin\\_hosp@126.com](mailto:yingmin_hosp@126.com) (Y.Z.),

[qingshun@nju.edu.cn](mailto:qingshun@nju.edu.cn) (Q.Z.),

[gmzhangyj@163.com](mailto:gmzhangyj@163.com) (G.Z.),

[lyx2186@shtrhospital.com](mailto:lyx2186@shtrhospital.com)

(X.L.)

<https://doi.org/10.1016/j.isci.2022.104042>



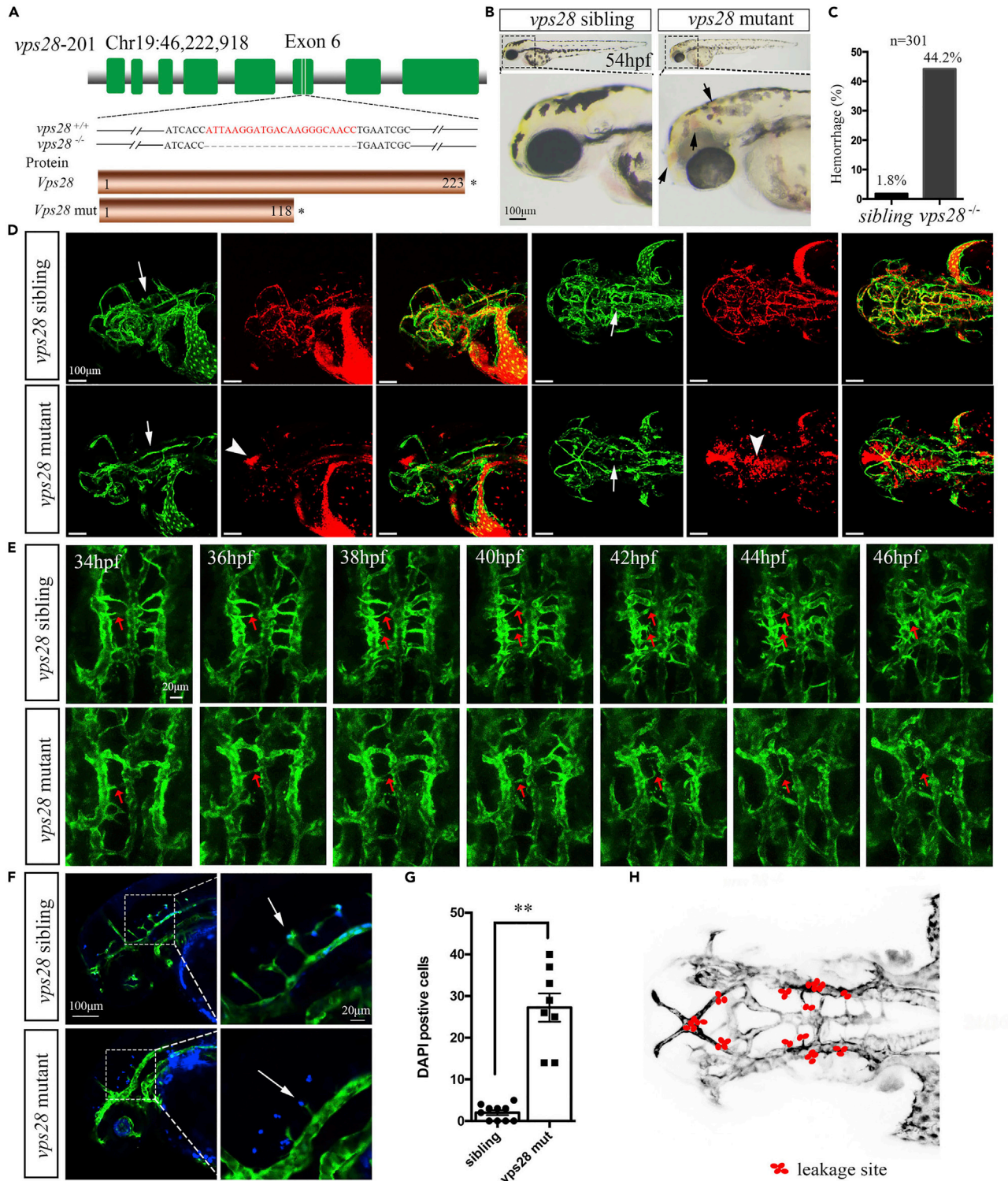


**Figure 1. *vps28* knockout displayed the abnormal angiogenesis of brain vascular CtAs in zebrafish larval**

(A) Schematic showed that the *vps28* mutant generated by the CRISPR/Cas9 system was with 22 bp deletion in exon 6, and the predicted *Vps28* mutant protein was shortened with only 118 amino acids.

(B) The phenotype of *vps28* mutant with intracranial hemorrhage (black arrows) in 54 hpf zebrafish larval. Scale bar: 100 μm.

(C) Proportion of the intracranial hemorrhage occurred in *vps28* mutants at 54 hpf.

**Figure 1. Continued**

- (D) Confocal images shown that *vps28* loss-of-function caused defective of CtAs formation (arrows) and blood cell leakage (arrowheads) in the brain of Tg (Kdrl: eGFP; Gata1: DsRed) larvae at 54 hpf. Scale bar: 100  $\mu$ m.
- (E) Confocal time-lapse shown that in *vps28* mutant the CtAs sprouting (arrows) and the connection of CtAs with BA was failed in live Tg (Kdrl: eGFP) embryos between 34 hpf and 46 hpf. Scale bar: 20  $\mu$ m.
- (F) Confocal images shown that *vps28* depleted embryos caused more DAPI-positive particles (blue) in the brain of Tg (Kdrl: eGFP) embryos at 54 hpf, the area outline by the rectangles in the left are enlarged in the right. Scale bar: 100  $\mu$ m (left) and 20  $\mu$ m (right).
- (G) Leakage of DAPI out of vascular in *vps28* mutants was counted.
- (H) Schematic shows the leakage site (red dots) in all 8 mutants as observed by confocal imaging. Green color represents the blood vessels (D, E, and F) and red color represents the red blood cell (D). Data are represented as mean  $\pm$  SD. \*\* $p < 0.01$ .

MVBs are intracellular single membrane-bound organelles that participate in a variety of biological processes, including protein trafficking, recycling, and degradation, as well as in the secretion of extracellular vesicles (EVs) (Gurunathan et al., 2019; Kalluri and LeBleu, 2020; Von Bartheld and Altick, 2011). MVB biogenesis is mediated by the endosomal sorting complex required for transport (ESCRT) complexes (Henne et al., 2011). The ESCRT system consists of four major subcomplexes: ESCRT-0, ESCRT-I, ESCRT-II, and ESCRT-III (Henne et al., 2011). Vacuolar protein sorting 28 (Vps28), which was first identified in yeast and is conserved in mammals and plants, is a component of the ESCRT-1 complex that regulates the MVB-dependent cargo sorting (Henne et al., 2011; Katzmann et al., 2001). Functional loss of Vps28 diminishes the endosomal trafficking of Awd in adipocytes of *Drosophila* larval (Mezzofanti et al., 2019). Vps28 is also expressed in neurons and is involved in the stabilization of dendrites in hippocampal neurons by regulating the activity of rapamycin complex 1 (Firkowska et al., 2019). Vps28 directly interacts with G $\beta$  $\gamma$  and regulates organization of mitotic spindles (Dionisio-Vicuna et al., 2018). Furthermore, VPS28A and VPS28B double mutants displayed obvious developmental defects in regulating vacuole formation and endosomal sorting of proteins in *Arabidopsis* (Liu et al., 2020). However, the involvement of Vps28 in the development of brain vascular remains undetermined.

In the present study, we demonstrate that Vps28 expressed by neurons regulates vascularization of the CNS by controlling the transfer of VEGF-A through the secretion of EVs. In Vps28-deleted zebrafish, the angiogenesis of CtAs was significantly disrupted and the BBB integrity was compromised, thereby causing severe intracranial hemorrhage. Interestingly, whole mount *in situ* hybridization of *vps28*, *vps28* transgenic line, and fluorescence-activated cell sorting (FACS) experiments indicated that *vps28* is mainly expressed in CNS neurons, suggesting that the CNS vascularization and communication is disturbed in Vps28 mutants. VPS28 loss-of-function dramatically decreased the secretion of EVs by influencing MVBs formation, both *in vitro* and *in vivo*. We further confirmed that EVs secreted by neurons contain VEGF-A and participated in the generation of CtAs. In summary, our study demonstrates that Vps28 plays a critical role in the vascularization of CNS by regulating the formation of MVBs and affecting the secretion of VEGF-A-containing EVs.

**RESULTS****Vps28 is required for the formation of cranial vasculature during angiogenesis**

VPS28 is enriched in neurons and plays crucial roles in neural development (Firkowska et al., 2019). To investigate whether Vps28 participates in the development of brain vasculature *in vivo*, we generated *vps28* mutants of zebrafish using the CRISPR/Cas9 technology, guided by a specific gRNA, targeting the *vps28* exon6 in the zebrafish genome. One *vps28* mutant allele with a 22 bp deletion in *vps28* was obtained. The *vps28* mutants encoded a truncated protein, terminated at the amino acid position 118 (Figure 1A), resulting in the lack of the conserved domain (40–220 aa) of the Vps28 superfamily; the relevant protein sequence of the wild type and the mutant Vps28 are presented in Figure S1. The *vps28* mutants appeared to be morphologically normal for up to 36 h postfertilization (hpf) (data not shown). However, they displayed decreased pigment granules and cranial hemorrhages at 54 hpf and the larvae became necrotic and died at 3 days postfertilization (dpf) (Figure 1B). Approximately 44.2% of the *vps28* mutants exhibited an obvious intracranial hemorrhage phenotype, whereas only 1.8% of the *vps28* siblings (comprising *vps28*<sup>+/+</sup> and *vps28*<sup>+/-</sup>) displayed spontaneous hemorrhage (Figure 1C).

To demonstrate whether *vps28* is essential for the brain vascular angiogenesis, *vps28* heterozygotes were crossed into the background of double transgenic zebrafish Tg (Kdrl: eGFP; Gata1: DsRed) background. In contrast to *vps28* siblings, DsRed-expressing blood cells were found to be accumulated in the brain of *vps28* mutants. In addition, *vps28*-deficient zebrafish embryos showed severe impairment of CtAs development (Figure 1D), whereas development of the other brain vascular and intersegmental vessels (ISVs) was normal (data not shown).

To further investigate the processes leading to these differences within the hindbrain vasculature, confocal time-lapse imaging analysis was performed in Tg (Kdrl: eGFP) zebrafish embryos. It was found that the growth of CtAs, sprouting from the PHBC and BA, was impaired, leading to failure in the formation of an elaborate network of CtAs in *vps28* mutants (Figure 1E). In addition, to determine whether the blood circulation is required for the CtAs formation in *vps28* mutants, a *tnnt2a* morpholino was used to generate the “silent heart” and “no blood flow” embryos (Sehnert et al., 2002). In *tnnt2a* mutants, in which red blood cells were accumulated in the trunk region, the formation of CtAs appeared normal in *tnnt2a* morphants compared with that in control and the deficit of angiogenesis in *vps28* mutants also occurred in the absence of circulation (Figure S2). These results suggested that the lack of CtAs development is primarily because of the defect in *Vps28* and not because of the deficiency of blood circulation.

Next, we investigated whether the intracranial hemorrhage in *vps28* mutant embryos was caused by the impairment of BBB function. The leakage tracer, 4',6-diamidino-2-phenylindole (DAPI), was microinjected into the circulatory system through the common cardinal vein (CCV) in Tg (Kdrl: eGFP) embryos at 54 hpf and the CNS vasculature in the embryos was then examined via confocal live imaging. The number of DAPI-positive parenchymal nuclei was used for quantification of the degree of blood leakage in the zebrafish brain (Tam et al., 2012; Xu et al., 2017). We found a significantly higher accumulation of DAPI-positive parenchymal cell nuclei in *vps28* mutant embryos compared with that in *vps28* siblings (Figures 1F and 1H). Based on the position of DAPI-positive parenchymal cell nuclei, we observed that the leakage across the BBB in *vps28* mutants was mainly concentrated in the PHBC, middle cerebral vein, and only a small amount of it occurred in the tip cells of deficient CtAs (Figure 1G). Overall, these results indicate that *Vps28* is essential for the angiogenesis of CtAs and for the integrity of the brain vasculature.

### Vps28 is enriched in neurons

To determine the function of *Vps28* in the development of CtAs, we first assessed the expression pattern of *Vps28* in zebrafish using whole mount *in situ* hybridization. *Vps28* was extensively expressed at 30% epiboly and was widely expressed at the somite stage. However, it was abundantly and specifically expressed in the CNS at 24 hpf and 48 hpf (Figure 2A). To better understand the function of *Vps28* in CNS angiogenesis, we constructed a Tg (*Vps28*: eGFP) transgenic zebrafish. GFP was expressed under the control of the *Vps28* promoter. We found that GFP was widely expressed at 30% epiboly and 5-somite stage, and was specifically expressed in the brain at 24 and 36 hpf, strictly mimicking the endogenous expression pattern of *vps28* (Figure 2B).

To ascertain the cellular localization of *Vps28* in the brain, Tg (*Vps28*: eGFP) zebrafish were crossed into the Tg (Kdrl: mCherry) background to verify whether *Vps28* was expressed in the ECs. We found that *Vps28* was strongly expressed throughout the brain in the Tg (*Vps28*: eGFP) embryos at 48 hpf (Figure 2D). Consistent with the *Vps28* expression pattern at 48 hpf, *vps28* was extensively expressed in the CNS at 72 hpf but not in the dorsal longitudinal vessel (DLV) and mesencephalic vein (MsV) (Figure 2E). Flow cytometry and real-time PCR analyses were performed to detect the enrichment of *vps28*. It was observed that *vps28* was more enriched in the neurons than in the ECs (Figure 2C). Furthermore, we observed robust *vps28* expression in primary cultures of G0 mouse cortical neurons (Tubb3<sup>+</sup>) (Figure 2F). To determine whether neuronal-derived *vps28* is involved in the CtAs angiogenesis, we directly microinjected *vps28*, under the control of an HuC promoter, into *vps28* mutants. The neuronal-derived *vps28* could partially rescue the defects in CtAs development (Figures 2G and 2H). Taken together, these results suggest that neuron-enriched *Vps28* might play an important role in CtAs angiogenesis in the brain vasculature.

### VPS28 knockdown inhibits EVs secretion *in vitro*

VPS28 belongs to the ESCRT family and is one of the subunits of the ESCRT-I complex that participates in the formation of MVBs and secretion of EVs (Henne et al., 2011). We sought to identify whether the abnormal angiogenesis of CtAs in *vps28* mutants was because of altered MVB formation and EVs secretion. We knocked down VPS28 in human embryonic kidneys (HEK) 293T cell line by transfecting an siRNA targeting VPS28. The efficiency of VPS28 siRNA knockdown was confirmed via western blot analysis (Figure 3A). Subsequently, we detected MVB formation in VPS28 knockdown HEK 293T cells using immunofluorescence. VPS28 knockdown resulted in a clustered localization of HGS, an MVB marker, as evidenced by

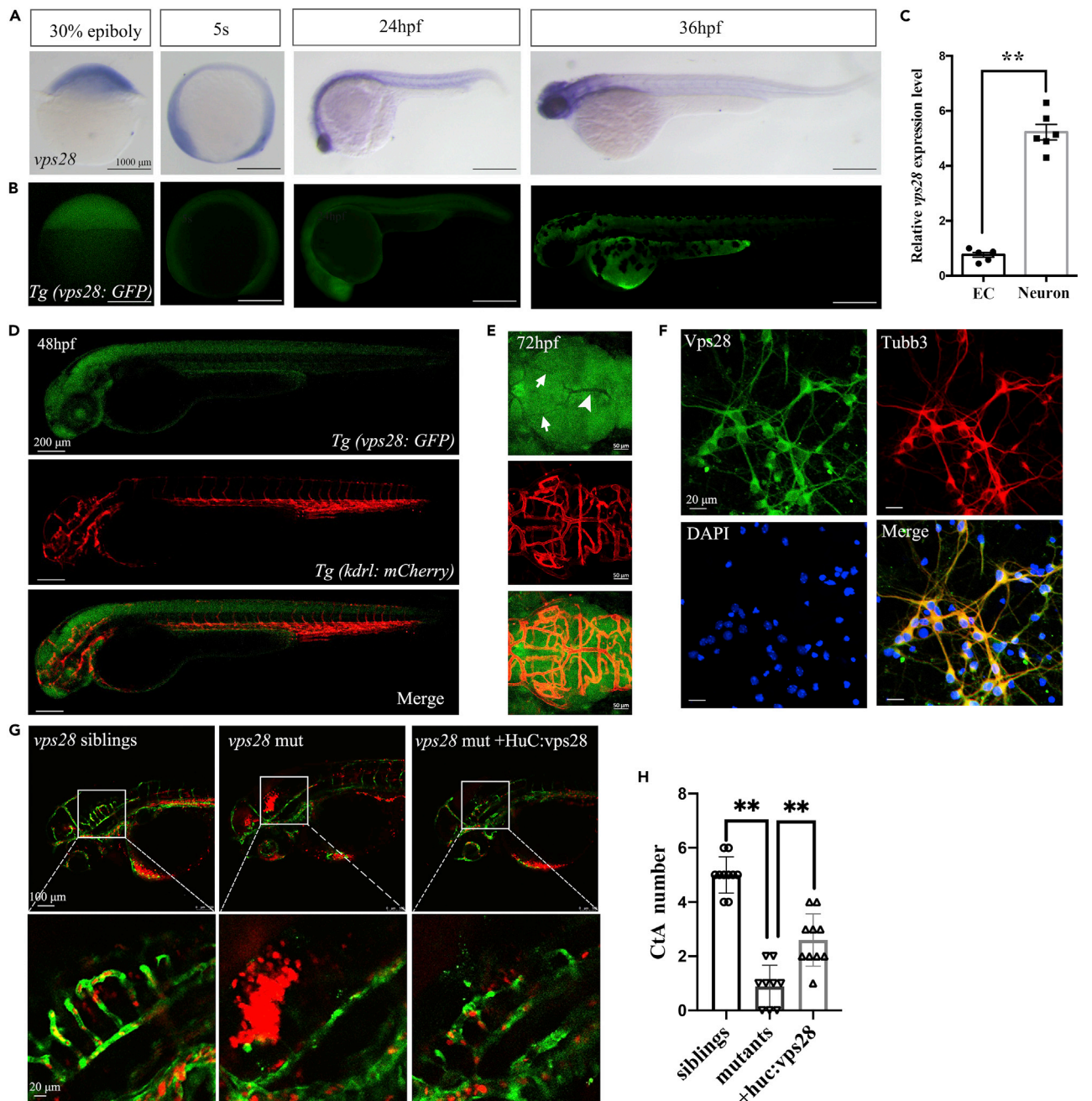


**Figure 2. Vps28 was enriched in CNS and cultured mouse cortical neurons**

(A) The expression pattern of *vps28* at 30% epiboly, 5-somite (5s), 24 hpf, and 36 hpf stage in zebrafish.

(B) Relative expression pattern of *vps28* in Tg (*Vps28: GFP*).

(C) Relative expression level of *vps28* in zebrafish ECs and neurons, which were sorted by flow cytometry from Tg (*Kdrl: eGFP*) and Tg (*Huc: eGFP*) embryos at 2 dpf, respectively.

(D and E) Expression of *vps28* in Tg (*vps28: eGFP; Kdrl: mCherry*) at 48 hpf and 72 hpf. *vps28* was mainly expressed in the zebrafish CNS than DLV (arrowhead) and MsV (arrow) at 72 hpf; DLV, dorsal longitudinal vein; MsV, Mesencephalic vein (E).

(F) Confocal images of primary mouse cortical neurons immunolabeled with Vps28 at 5 days in culture, a majority of the Tubb3 expressing neurons express detectable levels of Vps28 in primary mouse cortical neurons.

(G) Effects of *vps28* driven by the HuC promoter (*huc: vps28*) on CtAs defects of *vps28* mutants.

(H) Graphical representations of the CtAs numbers in (G). Data are represented as mean  $\pm$  SD. \*\**p* < 0.01.

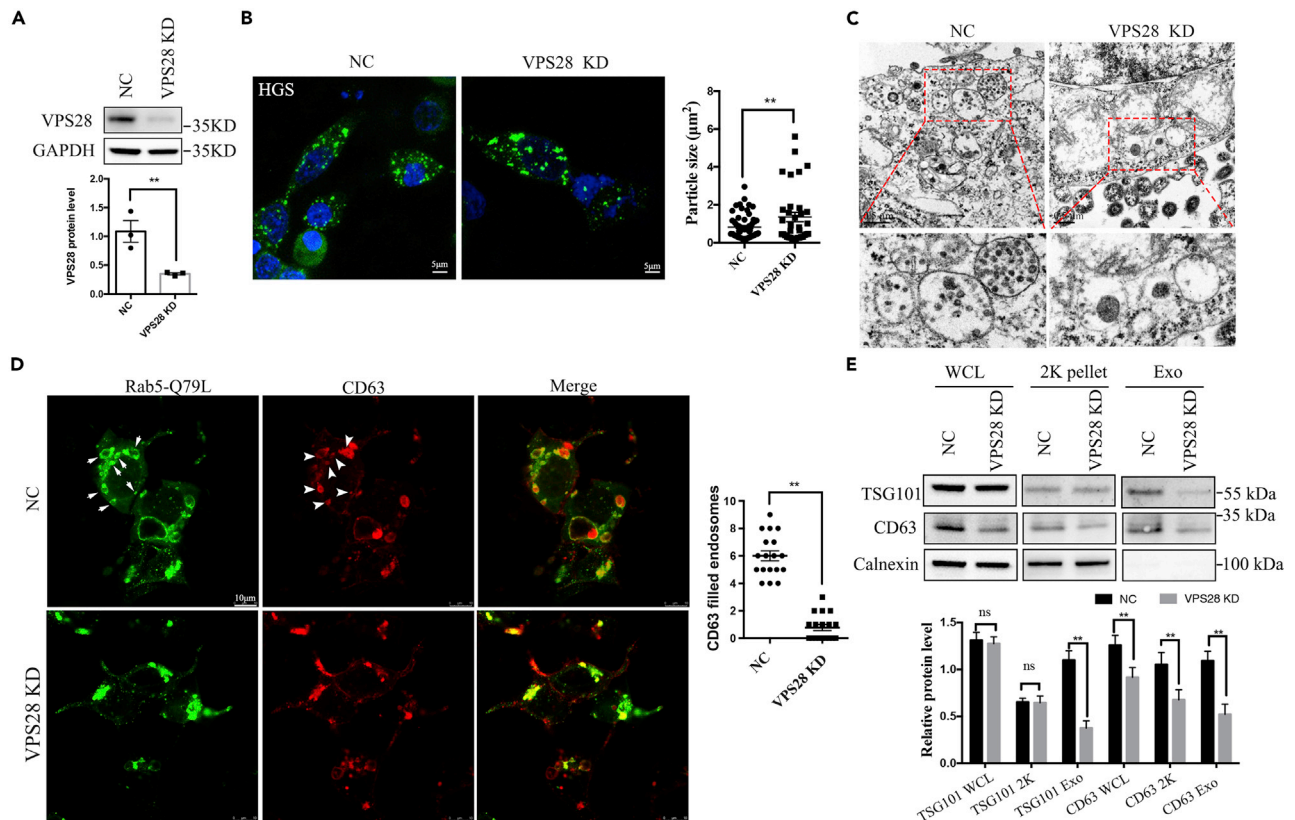


**Figure 3. VPS28 regulates secretion of EVs *in vitro***

(A) Western blot analysis of VPS28 knockdown efficiency by siRNA in 293T cell line.

(B) Confocal images analysis of the endosome markers HGS in 293T cells co-transfected with VPS28 negative control siRNA or VPS28 siRNA. Right graph, quantification of HGS + average particle size per cell. Scale bar, 5 µm.

(C) TEM analysis of representative fields with MVBs in 293T cells transfected with VPS28 negative control siRNA or VPS28 siRNA. The area outlined by the rectangles in the upper graph is enlarged in the lower graph. Scale bar, 0.5 µm.

(D) Confocal images analysis of CD63 (red) and Rab5-Q79L-GFP<sup>+</sup> endosomes (green) in control and VPS28 knockdown 293T cells. Right graph, number of endosomes per cell.

(E) Western blot analysis of EVs collected by ultracentrifugation from cell culture supernatants from control or VPS28 knockdown 293T cells. Cells, 2K centrifugation particles, and EVs (Exo) were blotted for the EVs markers TSG101, CD63, and for the endoplasmic reticulum marker Calnexin. Data are represented as mean ± SD. \*\*p < 0.01.

the increased size of HGS<sup>+</sup> particles in cells (Figure 3B). Transmission electron microscopy (TEM) analyses revealed significant reduction in the number and density of MVBs in VPS28 knockdown cells (Figure 3C).

To determine whether the decrease in the number of MVBs in VPS28 knockdown cells was influenced by the first step in MVB biogenesis, we transfected HEK 293T cells with the GTPase-defective mutant, Rab5(Q79L), which forms enlarged early and late endocytic endosomes (Stenmark et al., 1994; Villarroya-Beltri et al., 2016; Wegner et al., 2010). VPS28 knockdown dramatically affected the morphology of the MVBs and significantly decreased the number of endosomes compared with that in the negative control (Figure 3D).

Next, we attempted to ascertain whether the loss of function of VPS28 in HEK 293T cells would affect EVs secretion. The levels of EVs markers, CD63 and TSG101, were analyzed in whole cell lysates (WCL), 2K pellet, and purified EVs via western blot analysis. Knockdown of VPS28 in 293T cells led to a significant decrease in TSG101 levels in ultracentrifuged pellets, but not in the WCL and 2K pellet. However, a drastic reduction in CD63 levels was observed in the secreted EVs and 2K pellet, as well as in WCL. In addition, calnexin was abundant in the WCL and 2K pellet but was barely detected in pure EVs, indicating that the extracted EVs were relatively pure and were free of contamination from other cell compartments (Figure 3E). Taken together, these results suggest that, *in vitro*, VPS28 regulates the secretion of EVs by influencing the formation of MVBs.

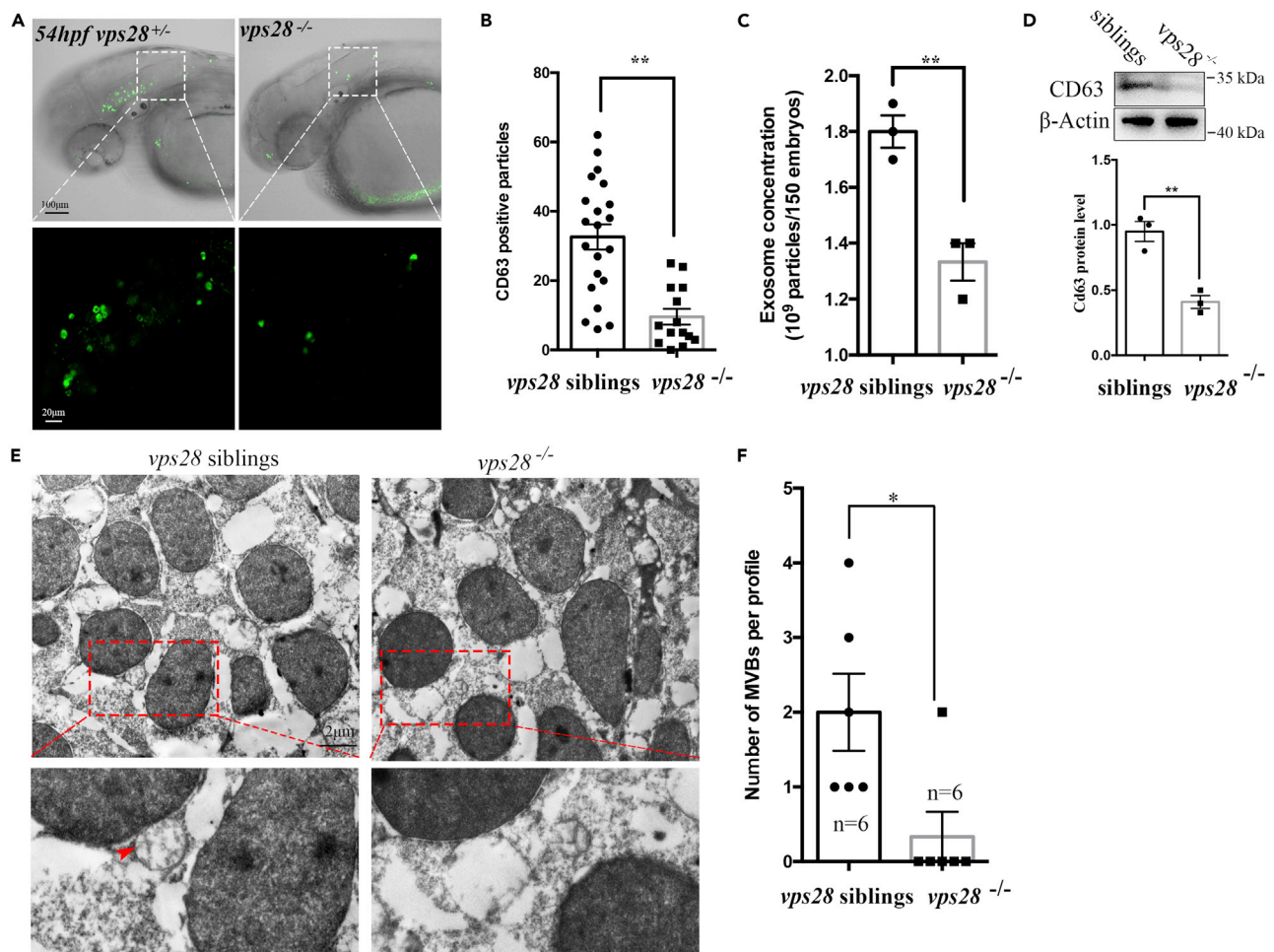


**Figure 4. Vps28 controlling the secretion of EVs in zebrafish**

(A) Confocal images analysis of CD63 positive particles in zebrafish CNS at 54 hpf. HuC:CD63-eGFP plasmids were microinjected into the 1-cell stage zebrafish *Vps28* mutants, the area outlined by the rectangles upper graph are enlarged in lower graph.

(B) CD63 positive particles were dramatically decreased in *vps28* knockout embryos.

(C) NTA analysis of total EVs concentration in 2.5 dpf *vps28* siblings and *vps28* mutants.

(D) Western analysis of EVs marker CD63 expression in 2.5 dpf *vps28* siblings and *vps28* depletion embryos.

(E) TEM analysis of representative fields with MVBs in *vps28* siblings and *vps28* depletion embryos at 54 hpf. The area outlined by the rectangles in the upper graph is enlarged in the lower graph. Scale bar, 2 μm.

(F) Quantification of MVB numbers in the fields of *vps28* siblings and *vps28* mutants (n = 6). Data are represented as mean ± SD. \*p < 0.05, \*\*p < 0.01.

### Vps28 knockout decreases EVs secretion *in vivo*

Next, we determined whether *in vivo* EVs secretion was disrupted in *Vps28* knockout mutants, in line with the results of the *in vitro* experiments. The neuron-specific distribution of CD63-enriched endosomes was detected in zebrafish embryos by transiently expression of CD63-GFP driven by the HuC promoter (HuC:CD63-GFP), which was used to visualize the fluorescent reporter CD63-GFP in EVs *in vivo* and the fusion of MVBs with the plasma membrane *in vitro* (Verweij et al., 2018; Xu et al., 2017). *In vivo* confocal imaging in zebrafish *Vps28* mutants transiently expressing HuC:CD63-GFP showed significantly decreased number of GFP-positive neuronal endosomes in the mutants compared with that in *Vps28* siblings (Figures 4A and 4B). The results suggest that *Vps28* may regulate CD63-filled endosomes. Next, we characterized the total number of EVs by dissociating 2.5 dpf-old *Vps28* mutants and control embryos, subjecting them to collagenase D treatment, and isolating EVs from the supernatant via ultracentrifugation (Verweij et al., 2019). Nanoparticle tracking analysis (NTA) of the ultracentrifuged particles revealed that the number of pellets secreted by *Vps28* knockout embryos was reduced compared with that in the control group (Figure 4C). Consistent with the NTA results, western blot analysis of the EVs marker CD63 revealed that

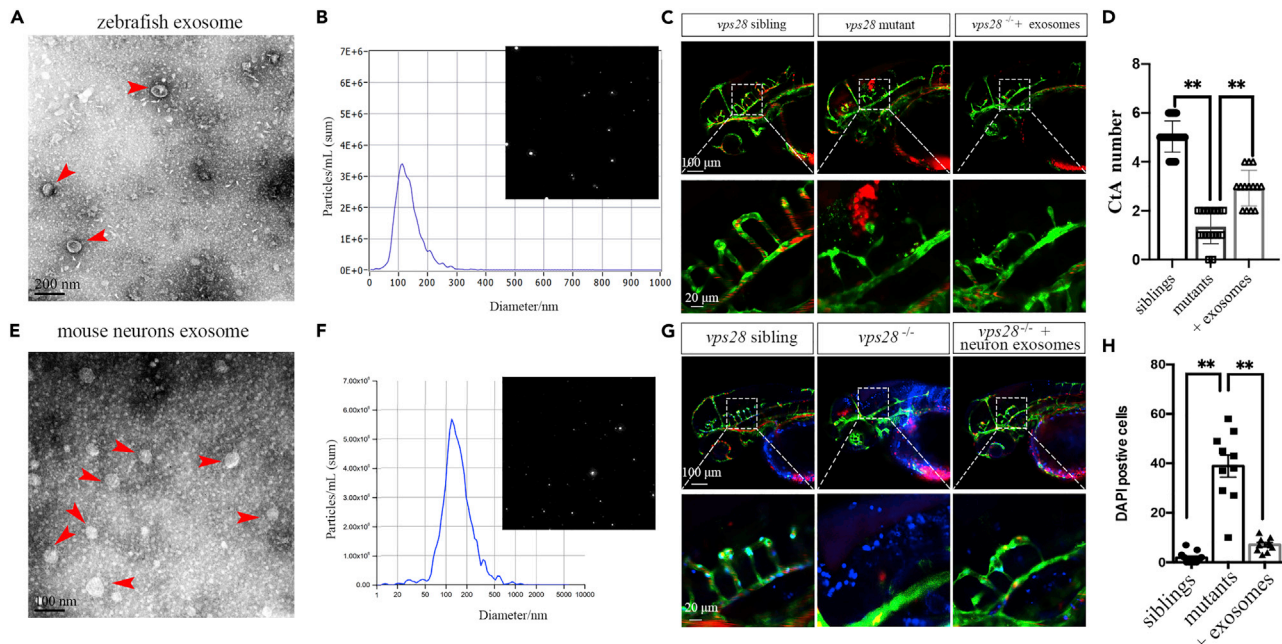


**Figure 5. Zebrafish and primary mouse cortical neurons-derived EVs could partially rescue the angiogenesis of CtAs in *vps28* mutants**

(A and B) Characterization of zebrafish-derived EVs by TEM and NTA in 54 hpf larvae. The arrowhead represents the classical EVs. (C) Zebrafish embryos-derived EVs microinjected into the CCV of zebrafish embryos could alleviate the CtAs defect in *vps28* mutants at 54 hpf. (D) Graphical representations of the CtAs numbers in (C). (E and F) Characterization of primary mouse cortical neurons derived EVs by TEM. The arrowhead represents the EVs. (G and H) Primary mouse cortical neurons-derived EVs microinjected into the CCV of zebrafish embryos could rescue the development of CtAs (G) and reduce the neurovascular DAPI leakage (H) in 54 hpf larvae. Data are represented as mean  $\pm$  SD. \* $p < 0.05$ .

knockout of *Vps28* in zebrafish led to a significant decrease in CD63 levels in the ultracentrifuged pellets but not in the WCL (Figure 4D), suggesting that *Vps28* significantly regulates the secretion of EVs *in vivo* by affecting the number of endosomes.

To further explore whether *Vps28* influences EV secretion by affecting the formation of MVBs *in vivo*, we performed a TEM analysis and determined the number and morphology of MVBs in zebrafish CNS. MVBs and intraluminal vesicles (ILVs) were relatively easy to observe in wild type embryos, but were almost undetectable in *Vps28*-depleted zebrafish embryos (Figure 4E). Moreover, the number of MVBs per cell decreased in *Vps28* mutant embryos compared with that in the control embryos (Figure 4F). Overall, these results indicate that, *in vivo*, *Vps28* regulates the secretion of EVs by influencing the formation of MVBs.

### EVs are involved in the formation of CtAs in the brain

EVs play a significant role in many aspects of cellular functions and pathological states, including angiogenesis, inflammation, immune responses, tissue homeostasis, neurodegenerative diseases, and cancer (Gurunathan et al., 2019; Howitt and Hill, 2016). In view of the impairment of the EVs secretion pathway in *Vps28* mutants, we hypothesized that neuronal EVs may participate in regulating vascular angiogenesis in the brain by delivering specific substances to ECs. To test this hypothesis, we first isolated EVs from the zebrafish whole embryos using gradient ultracentrifugation. TEM and NTA analysis of the purified pellets revealed saucer-type small membrane vesicles with an average diameter of  $113 \pm 77$  nm (mean  $\pm$  SD, Figures 5A and 5B), suggesting that they were EVs. Next, we transiently microinjected the isolated EVs into the CCV of Tg (Kdrl: eGFP) *vps28* mutants at 30 hpf to evaluate whether EVs played a significant role in brain vascularization. Injection of zebrafish EVs into the CCV partially promoted sprouting of CtAs from the PHBCs in the zebrafish brain at 54 hpf (Figures 5C and 5D). To further confirm whether neuronal EVs are involved in CtAs development, we extracted EVs from the conditioned medium of cultured primary mouse cortical neurons. Using TEM and NTA analyses of the purified pellets, EVs with an average diameter of  $127 \pm 80$  nm (mean  $\pm$  SD) were identified (Figures 5E and 5F). We microinjected the extracted neuronal EVs into the CCV of double transgenic zebrafish, Tg (Kdrl: eGFP; Gata1: DsRed) at 30 hpf and compared

the formation of parts of normal CtAs in *vps28* mutants with that in non-injected morphants (Figure 5G). Moreover, co-injection of DAPI into the circulation system of *Vps28* mutants at 54 hpf followed by counting of DAPI-positive nuclei of brain parenchymal cells showed that a reduced count of DAPI-positive nuclei was observed in the neuronal EVs rescued group compared with that in the *vps28* mutant group (Figure 5H). These results indicated that EVs play an important role in CtAs development and in alleviating the hemorrhagic phenotype in *vps28* mutants.

### EVs containing VEGF-A participate in regulating brain vascular angiogenesis

VEGF signaling plays an important role in the development of the vascular system by regulating the vascular specification and differentiation (Jin et al., 2017). The decrease in CtAs sprouts in *Vegfa*-deficient zebrafish embryos during cerebrovascular development was akin to the deficiency in CtAs formation in the brains of *Vps28* mutants. Moreover, it has been reported that astrocyte-derived VEGF-A is involved in the homeostatic maintenance of the BBB homeostasis (Argaw et al., 2012). Therefore, we hypothesized that EVs may transfer VEGF-A from neurons to ECs, thereby controlling the vascularization of CNS. To test this hypothesis, we first detected the expression of VEGF-A in cultured primary cortical neurons. Immunofluorescence analysis showed robust VEGF-A expression, indicating that VEGF-A is abundant in the nervous system (Figure 6A). Furthermore, the presence of VEGF-A was also observed in EVs isolated from the cell supernatant of cultured primary cortical neurons (Figure 6B). These results indicated that neuronal EVs can transfer VEGF-A in the CNS.

To demonstrate whether VEGF-A-containing EVs in the circulatory system are involved in brain angiogenesis, we transiently microinjected human VEGF-A-121 into the CCV of Tg (Kdrl: eGFP) zebrafish embryos at the onset of the CtAs sprouting stage. Confocal imaging revealed that VEGF-A-121 partially rescued the abnormal CtAs formation (Figure 6C). Moreover, overexpression of VEGF-A-121 dramatically decreased the intracranial hemorrhage, as evidenced by reduced DAPI leakage (Figures 6C and 6D). Likewise, overexpression in the EVs extracted from zebrafish embryos also alleviated the CtAs deficiency (Figures 6E and 6F). More importantly, the VEGF-A mRNA and protein levels in *Vps28*-depleted embryos were similar to those in *Vps28* siblings (Figures 6G and 6H), but the levels were significantly diminished in the EVs of *Vps28* (Figure 6I). In addition, we microinjected the EVs extracted from wild type zebrafish into the Tg (Kdrl: eGFP; Gata1: DsRed) zebrafish embryos at 1-cell stage and observed that the formation of CtAs in *vps28* mutants was almost normal compared with that in uninjected mutants (Figures 6J and 6K). However, when VEGF signaling was blocked with *vegfaa* MO, the formation of CtAs did not differ between *vps28* mutants and microinjected with *vegfaa* morphants-extracted EVs (Figures 6J and 6K). Collectively, these results indicate that the expression of VEGF in EVs is important for hindbrain CtAs angiogenesis and mediates the neurovascular crosstalk in the CNS.

### DISCUSSION

As opposed to the classical VEGF signaling pathway that regulates angiogenesis in the CNS, our study demonstrates that the ESCRT-1 complex subunit, *Vps28*, which is abundantly expressed in the nervous system, affects angiogenesis of CtAs through the secretion of VEGF-A-containing EVs by influencing the generation of MVBs (Figure 6L). It highlights the function of the neuron–VEGF–EVs–EC–angiogenesis axis in neurovascular communication.

*Vps28*, which belongs to class E VPS proteins and participates in the ESCRT-I complex, is localized in ubiquitin-rich endosomes and is required for receptor trafficking (Bishop et al., 2002). In addition, *Vps28* plays an important role in embryogenesis by regulating cell-division patterns in plant development (Liu et al., 2020). In the present study, *Vps28* knockout via the CRISP/Cas9 system in zebrafish resulted in significant intracranial hemorrhage at 48 hpf, probably because of the disruption of cerebrovascular integrity, leading to larval mortality at approximately 80 hpf. Interestingly, *vps28* mutants displayed normal angiogenesis of ISV from the DA. This phenotype demonstrated that different mechanisms govern brain vascular angiogenesis and ISV angiogenesis in *Vps28* null-allele embryos.

An extensive body of evidences suggests that angiogenesis is temporally coordinated with the barriergenesis (Engelhardt and Liebner, 2014; Umans et al., 2017), *Prnd* is involved in blood vessel development and endothelial barrier integrity in the CNS (Chen et al., 2020), and CTGF participates in both retinal angiogenesis and BBB (Moon et al., 2020). Neurons and glia also play important roles in coupled angiogenesis and

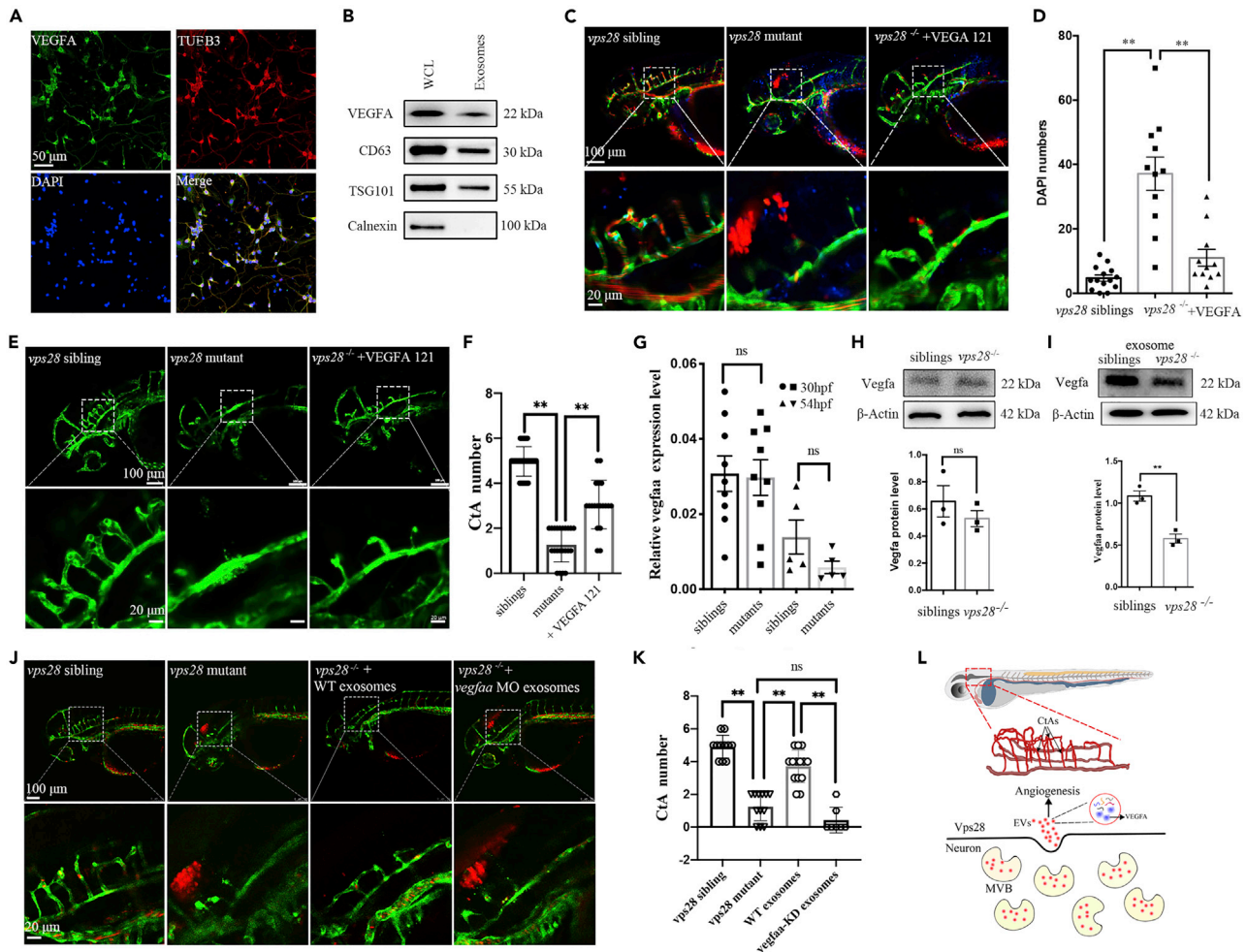


**Figure 6. Neuronal EVs contained VEGFA are involved in brain vascular angiogenesis**

(A) Confocal images analysis of VEGF-A expression in mouse primary cortical neurons at 5 days in culture.  
 (B) Western blot identification of the EVs derived VEGF-A in mouse primary cortical neurons.  
 (C) Confocal images analysis of rescued-intracerebral-hemorrhage phenotype in VEGF-121 microinjected *vps28* mutants in 54 hpf Tg (Kdrl: eGFP; Gata1: DsRed) larvae.  
 (D) Statistical analysis of DAPI leakage in the VEGF-121 injected embryos corresponding to (C).  
 (E) Confocal images analysis of CtAs branching in VEGF-121 injected embryos at 54 hpf.  
 (F) Graphical representations of the CtAs numbers in (E).  
 (G) qPCR analysis of the *vegfaa* expression level in *vps28* mutants and siblings at 30 hpf and 54 hpf.  
 (H) Western blot analysis of *Vegfa* protein level in *vps28* depleted embryos compared with *vps28* siblings in the whole embryos.  
 (I) Western blot analysis of *Vegfa* protein level in EVs of the 54 hpf *vps28* mutants compared with relative *vps28* siblings.  
 (J) Effects of *vegfaa* specific deleted exosomes on *vps28* mutants CtAs angiogenesis at 54 hpf.  
 (K) Graphical representations of the CtAs numbers in (J). Data are represented as mean  $\pm$  SD. \*\* $p < 0.01$ .  
 (L) Vps28 working model. Vps28 is highly expressed in neurons and participates in neurovascular communication by controlling the secretion of neuronal EVs.

barriergenesis (Biswas et al., 2020). We found that depletion of *vps28* caused DAPI-leakage in CNS and defects in the development of CtAs; however, whether *vps28* regulates vascular barrier differentiation needs to be further investigated.

In vertebrates, CNS vessel growth and maturation is largely mediated by neural and vascular communication (Biswas et al., 2020; Paredes et al., 2018). An impairment of neural Tgfr2 secretion inhibits EC migration and reduces branching in angiogenesis (Hellbach et al., 2014). Here, we demonstrated that the expression of *Vps28* is higher in the CNS than in the ECs, suggesting that neuron-derived *Vps28* has

a non-cell-autonomous function in controlling the sprouting of the CtAs. However, it is important to determine whether the lower expression of Vps28 in the ECs can also regulate brain vascular development in the brain.

EVs, with diameter ranging from 50 to 200 nm, have a cup-shaped structure and originate intracellularly from endosomes. EVs are generated from MVBs containing cargo-laden ILVs. MVBs fuse with the plasma membrane of various cell types, following which the ILVs are secreted as EVs (van Niel et al., 2018). The ESCRT consists of five distinct protein complexes, ESCRT-0, ESCRT-I, ESCRT-II, ESCRT-III, and AAA ATPase Vps4 complex, which play important roles in MVB morphogenesis and synthesis of EVs (Henne et al., 2011, 2013). Depletion of the TSG101 and Hrs (ESCRT-0 protein), STAM1 (ESCRT-I protein), or CHMP6, ALIX (ESCRT-III) decreased the secretion of EVs (Gurunathan et al., 2019; Larios et al., 2020). Vps28 belongs to the ESCRT-I family that is involved in the intracellular trafficking of proteins and MVB formation (Firkowska et al., 2019; Mezzofanti et al., 2019). Nevertheless, the function of Vps28 in the secretion of EVs has not yet been elucidated. We found that VPS28 regulates the secretion of CD63-enriched EVs by mediating the formation of MVBs in an ESCRT-dependent manner both *in vitro* and *in vivo*. Our research uncovers the functions of the ESCRT-I protein, Vps28, in addition, we show that it is involved in the generation of EVs and plays an essential role in neural regulation during the formation of the brain vasculature.

During development of the brain vasculature, a few neural tissues secreting EVs were reported to promote CNS vascular formation. By delivering their cargo comprising miR-132, neuron-derived EVs contribute to the regulation of the BBB integrity in the vascular development in the zebrafish brain (Xu et al., 2017). This prompted us to determine whether defective CtA formation in *vps28* mutants was caused by the interruption of EV delivery. We harvested EVs from zebrafish whole embryos and from cultured mouse cortical neurons, microinjected them EVs into the 1-cell stage embryos or into the blood circulation system of 30 hpf zebrafish embryos through the CCV, and found that parts of CtAs could be rescued in *vps28* mutants. Interestingly, the mouse neuron-derived EVs were more effective in promoting brain angiogenesis and preventing blood leakage.

Neural-derived VEGF-A plays a critical role in brain angiogenesis. VEGF-A secreted from astrocytes is required for retinal vasculature angiogenesis and BBB formation (Argaw et al., 2012; Bozoyan et al., 2012; Scott et al., 2010). In the present study, we detected that the VEGF-A mRNA and protein levels in *vps28* mutants were not significantly different from those in *vps28* siblings. However, the VEGF-A protein levels in *vps28* mutant-derived EVs were dramatically lower than that in EVs from *vps28* siblings. In addition, direct injection of the VEGF121 protein into the CCV was able to partially rescue the CtAs angiogenesis and prevented vascular leakage in the brain. Furthermore, EVs derived from *vegfaa* morphants could not promote the angiogenesis of CNS. In summary, we demonstrated that Vps28 is enriched in the CNS and executes a non-cell-autonomous function in controlling the angiogenesis of the CtAs via transfer of VEGF-A-containing EVs to ECs.

### Limitations of the study

In our study, we found that *vps28* participated in the angiogenesis of CtAs and the integrity of BBB in zebrafish. We show that the *vps28* is involved in the development of CtAs by regulating the EVs secretion of VEGF. However, the mechanism through which *vps28* regulates the integrity of BBB needs to be further studied.

### STAR★METHODS

Detailed methods are provided in the online version of this paper and include the following:

- KEY RESOURCES TABLE
- RESOURCE AVAILABILITY
  - Lead contact
  - Materials availability
  - Data and code availability
- EXPERIMENTAL MODEL AND SUBJECT DETAILS
  - Zebrafish
  - Mouse primary cortical neuron culture and 293 T cell culture

● **METHODS DETAILS**

- Mutation and transgenic lines
- Flow cytometry, RNA extracted, real-time PCR and whole mount *in situ* hybridizations
- Transfection with siRNAs and plasmids in 293T cell
- EVs collection from *in vitro* cultured 293T cell, primary cortical neuron and zebrafish embryos
- Microinjection of plasmid, morpholino, EVs, VEGF-A and DAPI into zebrafish embryos
- Plasmid construction
- Immunofluorescence
- Western blot
- NTA measurement
- Confocal imaging
- Transmission electron microscopy

● **QUANTIFICATION AND STATISTICAL ANALYSIS**

**SUPPLEMENTAL INFORMATION**

Supplemental information can be found online at <https://doi.org/10.1016/j.isci.2022.104042>.

**ACKNOWLEDGMENTS**

This work was supported by the National Natural Science Foundation of China under Grant no. 81801503 and 81800284, Natural Science Foundation of Jiangsu Province under Grant no. BK20180286 and BK20180144, Natural Science Foundation of Shanghai under Grant no. 22ZR1457100 and 20ZR1451900, Scientific Research Project of Shanghai Health Committee under Grant no. 201740009, and Taizhou Science and Technology Support Plan (Social Development) project under Grant no. SSF20200345. We thank Prof. Jiulin Du for providing plasmid of HuC:CD63-GFP. We also thank Prof. Jingjing Zhang for the helpful advice on this project.

**AUTHOR CONTRIBUTIONS**

X.D., Y.Z., G.Z., and X.L. designed the project and edited the manuscript. Q.Z. supported the *vps28* mutants and provided the idea of the subject. X.D., D.J., and L.W. performed the experiment and wrote the manuscript. Y.H., X.W., and Y.Z. performed the experiment. L.Y. and J.Z. helped to identify the *vps28* mutants.

**DECLARATION OF INTERESTS**

The authors declare no competing interests.

Received: August 20, 2021

Revised: January 27, 2022

Accepted: March 4, 2022

Published: April 15, 2022

**REFERENCES**

- Argaw, A.T., Asp, L., Zhang, J., Navrazhina, K., Pham, T., Mariani, J.N., Mahase, S., Dutta, D.J., Seto, J., Kramer, E.G., et al. (2012). Astrocyte-derived VEGF-A drives blood-brain barrier disruption in CNS inflammatory disease. *J. Clin. Invest.* 122, 2454–2468. <https://doi.org/10.1172/JCI60842>.
- Bishop, N., Horman, A., and Woodman, P. (2002). Mammalian class E vps proteins recognize ubiquitin and act in the removal of endosomal protein-ubiquitin conjugates. *J. Cell Biol.* 157, 91–101. <https://doi.org/10.1083/jcb.200112080>.
- Biswas, S., Cottarelli, A., and Agalliu, D. (2020). Neuronal and glial regulation of CNS angiogenesis and barrierogenesis. *Development* 147, dev182279. <https://doi.org/10.1242/dev.182279>.
- Bohdanowicz, M., Balkin, D.M., De Camilli, P., and Grinstein, S. (2012). Recruitment of OCRL and Inpp5B to phagosomes by Rab5 and APPL1 depletes phosphoinositides and attenuates Akt signaling. *Mol. Biol. Cell* 23, 176–187. <https://doi.org/10.1091/mbc.E11-06-0489>.
- Bozoyan, L., Khghatyan, J., and Saghatelian, A. (2012). Astrocytes control the development of the migration-promoting vasculature scaffold in the postnatal brain via VEGF signaling. *J. Neurosci.* 32, 1687–1704. <https://doi.org/10.1523/JNEUROSCI.5531-11.2012>.
- Chen, Z., Morales, J.E., Avci, N., Guerrero, P.A., Rao, G., Seo, J.H., and McCarty, J.H. (2020). The vascular endothelial cell-expressed prion protein doppel promotes angiogenesis and blood-brain barrier development. *Development* 147, dev193094. <https://doi.org/10.1242/dev.193094>.
- Daneman, R., and Prat, A. (2015). The blood-brain barrier. *Cold Spring Harb. Perspect. Biol.* 7, a020412. <https://doi.org/10.1101/cshperspect.a020412>.
- Dionisio-Vicuna, M.N., Gutierrez-Lopez, T.Y., Adame-Garcia, S.R., Vazquez-Prado, J., and Reyes-Cruz, G. (2018). VPS28, an ESCRT-I protein, regulates mitotic spindle organization via Gbetagamma, EG5 and TPX2. *Biochim. Biophys. Acta Mol. Cell Res* 1865, 1012–1022. <https://doi.org/10.1016/j.bbamcr.2018.03.005>.
- Dong, X., Li, J., He, L., Gu, C., Jia, W., Yue, Y., Li, J., Zhang, Q., Chu, L., and Zhao, Q. (2017).

- Zebrafish Znf1 proteins control the expression of *hoxb1b* gene in the posterior neuroectoderm by acting upstream of *pou5f3* and *sall4* genes. *J. Biol. Chem.* 292, 13045–13055. <https://doi.org/10.1074/jbc.M117.777094>.
- Dong, Z., Dong, X., Jia, W., Cao, S., and Zhao, Q. (2014). Improving the efficiency for generation of genome-edited zebrafish by labeling primordial germ cells. *Int. J. Biochem. Cell Biol.* 55, 329–334. <https://doi.org/10.1016/j.biocel.2014.08.020>.
- Engelhardt, B., and Liebner, S. (2014). Novel insights into the development and maintenance of the blood-brain barrier. *Cell Tissue Res.* 355, 687–699. <https://doi.org/10.1007/s00441-014-1811-2>.
- Firkowska, M., Macias, M., and Jaworski, J. (2019). ESCRT proteins control the dendritic morphology of developing and mature hippocampal neurons. *Mol. Neurobiol.* 56, 4866–4879. <https://doi.org/10.1007/s12035-018-1418-9>.
- Gerhardt, H., Golding, M., Fruttiger, M., Ruhrberg, C., Lundkvist, A., Abramsson, A., Jeltsch, M., Mitchell, C., Alitalo, K., Shima, D., and Betsholtz, C. (2003). VEGF guides angiogenic sprouting utilizing endothelial tip cell filopodia. *J. Cell Biol.* 161, 1163–1177. <https://doi.org/10.1083/jcb.200302047>.
- Gore, A.V., Monzo, K., Cha, Y.R., Pan, W., and Weinstein, B.M. (2012). Vascular development in the zebrafish. *Cold Spring Harb. Perspect. Med.* 2, a006684. <https://doi.org/10.1101/cshperspect.a006684>.
- Gurunathan, S., Kang, M.H., Jeyaraj, M., Qasim, M., and Kim, J.H. (2019). Review of the isolation, characterization, biological function, and multifarious therapeutic approaches of exosomes. *Cells* 8, 307. <https://doi.org/10.3390/cells8040307>.
- Hellbach, N., Weise, S.C., Vezzali, R., Wahane, S.D., Heidrich, S., Roidl, D., Pruszek, J., Esser, J.S., and Vogel, T. (2014). Neural deletion of *Tgfb2* impairs angiogenesis through an altered secretome. *Hum. Mol. Genet.* 23, 6177–6190. <https://doi.org/10.1093/hmg/ddu338>.
- Henne, W.M., Buchkovich, N.J., and Emr, S.D. (2011). The ESCRT pathway. *Dev. Cell* 21, 77–91. <https://doi.org/10.1016/j.devcel.2011.05.015>.
- Henne, W.M., Stenmark, H., and Emr, S.D. (2013). Molecular mechanisms of the membrane sculpting ESCRT pathway. *Cold Spring Harb. Perspect. Biol.* 5, a016766. <https://doi.org/10.1101/cshperspect.a016766>.
- Himmels, P., Paredes, I., Adler, H., Karakatsani, A., Luck, R., Marti, H.H., Ermakova, O., Rempel, E., Stoeckli, E.T., and Ruiz de Almodovar, C. (2017). Motor neurons control blood vessel patterning in the developing spinal cord. *Nat. Commun.* 8, 14583. <https://doi.org/10.1038/ncomms14583>.
- Howitt, J., and Hill, A.F. (2016). Exosomes in the pathology of neurodegenerative diseases. *J. Biol. Chem.* 291, 26589–26597. <https://doi.org/10.1074/jbc.R116.757955>.
- Isogai, S., Horiguchi, M., and Weinstein, B.M. (2001). The vascular anatomy of the developing zebrafish: an atlas of embryonic and early larval development. *Dev. Biol.* 230, 278–301. <https://doi.org/10.1006/dbio.2000.9995>.
- James, J.M., Gewolb, C., and Bautch, V.L. (2009). Neurovascular development uses VEGF-A signaling to regulate blood vessel ingression into the neural tube. *Development* 136, 833–841. <https://doi.org/10.1242/dev.028845>.
- Jin, D., Zhu, D., Fang, Y., Chen, Y., Yu, G., Pan, W., Liu, D., Li, F., and Zhong, T.P. (2017). Vegfa signaling regulates diverse artery/vein formation in vertebrate vasculatures. *J. Genet. Genomics* 44, 483–492. <https://doi.org/10.1016/j.jgg.2017.07.005>.
- Kalluri, R., and LeBleu, V.S. (2020). The biology, function, and biomedical applications of exosomes. *Science* 367, eaau6977. <https://doi.org/10.1126/science.aau6977>.
- Katzmann, D.J., Babst, M., and Emr, S.D. (2001). Ubiquitin-dependent sorting into the multivesicular body pathway requires the function of a conserved endosomal protein sorting complex, ESCRT-I. *Cell* 106, 145–155.
- Kimmel, C.B., Ballard, W.W., Kimmel, S.R., Ullmann, B., and Schilling, T.F. (1995). Stages of embryonic development of the zebrafish. *Dev. Dyn.* 203, 253–310. <https://doi.org/10.1002/aja.1002030302>.
- Langen, U.H., Ayloo, S., and Gu, C. (2019). Development and cell biology of the blood-brain barrier. *Annu. Rev. Cell Dev. Biol.* 35, 591–613. <https://doi.org/10.1146/annurev-cellbio-100617-062608>.
- Larios, J., Mercier, V., Roux, A., and Gruenberg, J. (2020). ALIX- and ESCRT-III-dependent sorting of tetraspanins to exosomes. *J. Cell Biol.* 219, e201904113. <https://doi.org/10.1083/jcb.201904113>.
- Liu, J., Wang, Y., and Cheng, Y. (2020). The ESCRT-I components VPS28A and VPS28B are essential for auxin-mediated plant development. *Plant J.* 104, 1617–1634. <https://doi.org/10.1111/tpj.15024>.
- Madelaine, R., Sloan, S.A., Huber, N., Notwell, J.H., Leung, L.C., Skariah, G., Halluin, C., Pasca, S.P., Bejerano, G., Krasnow, M.A., et al. (2017). MicroRNA-9 couples brain neurogenesis and angiogenesis. *Cell Rep.* 20, 1533–1542. <https://doi.org/10.1016/j.celrep.2017.07.051>.
- Matsuoka, R.L., Rossi, A., Stone, O.A., and Stainier, D.Y.R. (2017). CNS-resident progenitors direct the vascularization of neighboring tissues. *Proc. Natl. Acad. Sci. U S A* 114, 10137–10142. <https://doi.org/10.1073/pnas.1619300114>.
- Mezzofanti, E., Ignesti, M., Hsu, T., Gargiulo, G., and Cavaliere, V. (2019). Vps28 is involved in the intracellular trafficking of Awd, the Drosophila homolog of NME1/2. *Front Physiol.* 10, 983. <https://doi.org/10.3389/fphys.2019.00983>.
- Moon, S., Lee, S., Caesar, J.A., Pruchenko, S., Leask, A., Knowles, J.A., Sinon, J., and Chaquour, B. (2020). A CTGF-YAP regulatory pathway is essential for angiogenesis and barrierogenesis in the retina. *iScience* 23, 101184. <https://doi.org/10.1016/j.isci.2020.101184>.
- Nasevicius, A., Larson, J., and Ekker, S.C. (2000). Distinct requirements for zebrafish angiogenesis revealed by a VEGF-A morphant. *Yeast* 17, 294–301. [https://doi.org/10.1002/1097-0061\(200012\)17:4<294::AID-YEA54>3.0.CO;2-5](https://doi.org/10.1002/1097-0061(200012)17:4<294::AID-YEA54>3.0.CO;2-5).
- Obermeier, B., Daneman, R., and Ransohoff, R.M. (2013). Development, maintenance and disruption of the blood-brain barrier. *Nat. Med.* 19, 1584–1596. <https://doi.org/10.1038/nm.3407>.
- Paredes, I., Himmels, P., and Ruiz de Almodovar, C. (2018). Neurovascular communication during CNS development. *Dev. Cell* 45, 10–32. <https://doi.org/10.1016/j.devcel.2018.01.023>.
- Scott, A., Powner, M.B., Gandhi, P., Clarkin, C., Gutmann, D.H., Johnson, R.S., Ferrara, N., and Fruttiger, M. (2010). Astrocyte-derived vascular endothelial growth factor stabilizes vessels in the developing retinal vasculature. *PLoS One* 5, e11863. <https://doi.org/10.1371/journal.pone.0011863>.
- Sehnert, A.J., Huq, A., Weinstein, B.M., Walker, C., Fishman, M., and Stainier, D.Y. (2002). Cardiac troponin T is essential in sarcomere assembly and cardiac contractility. *Nat. Genet.* 31, 106–110. <https://doi.org/10.1038/ng875>.
- Stenmark, H., Parton, R.G., Steele-Mortimer, O., Lutcke, A., Gruenberg, J., and Zerial, M. (1994). Inhibition of rab5 GTPase activity stimulates membrane fusion in endocytosis. *EMBO J.* 13, 1287–1296.
- Tam, S.J., Richmond, D.L., Kaminker, J.S., Modrusan, Z., Martin-McNulty, B., Cao, T.C., Weimer, R.M., Carano, R.A., van Bruggen, N., and Watts, R.J. (2012). Death receptors DR6 and TROY regulate brain vascular development. *Dev. Cell* 22, 403–417. <https://doi.org/10.1016/j.devcel.2011.11.018>.
- Ulrich, F., Ma, L.H., Baker, R.G., and Torres-Vazquez, J. (2011). Neurovascular development in the embryonic zebrafish hindbrain. *Dev. Biol.* 357, 134–151. <https://doi.org/10.1016/j.ydbio.2011.06.037>.
- Umans, R.A., Henson, H.E., Mu, F., Parupalli, C., Ju, B., Peters, J.L., Lanham, K.A., Plavicki, J.S., and Taylor, M.R. (2017). CNS angiogenesis and barrierogenesis occur simultaneously. *Dev. Biol.* 425, 101–108. <https://doi.org/10.1016/j.ydbio.2017.03.017>.
- van Niel, G., D’Angelo, G., and Raposo, G. (2018). Shedding light on the cell biology of extracellular vesicles. *Nat. Rev. Mol. Cell Biol.* 19, 213–228. <https://doi.org/10.1038/nrm.2017.125>.
- Verweij, F.J., Bebelman, M.P., Jimenez, C.R., Garcia-Vallejo, J.J., Janssen, H., Neefjes, J., Knol, J.C., de Goeij-de Haas, R., Piersma, S.R., Baglio, S.R., et al. (2018). Quantifying exosome secretion from single cells reveals a modulatory role for GPCR signaling. *J. Cell Biol.* 217, 1129–1142. <https://doi.org/10.1083/jcb.201703206>.
- Verweij, F.J., Revenu, C., Arras, G., Dingli, F., Loew, D., Pegtel, D.M., Follain, G., Allio, G., Goetz, J.G.,

Zimmermann, P., et al. (2019). Live tracking of inter-organ communication by endogenous exosomes *in vivo*. *Dev. Cell* 48, 573–589.e574. <https://doi.org/10.1016/j.devcel.2019.01.004>.

Villarroya-Beltri, C., Baixauli, F., Mittelbrunn, M., Fernandez-Delgado, I., Torralba, D., Moreno-Gonzalo, O., Baldanta, S., Enrich, C., Guerra, S., and Sanchez-Madrid, F. (2016). ISGylation controls exosome secretion by promoting lysosomal degradation of MVB proteins. *Nat. Commun.* 7, 13588. <https://doi.org/10.1038/ncomms13588>.

Von Bartheld, C.S., and Altick, A.L. (2011). Multivesicular bodies in neurons: distribution, protein content, and trafficking functions. *Prog. Neurobiol.* 93, 313–340. <https://doi.org/10.1016/j.pneurobio.2011.01.003>.

Wagenaar, T.R., Tolstykh, T., Shi, C., Jiang, L., Zhang, J., Li, Z., Yu, Q., Qu, H., Sun, F., Cao, H., et al. (2015). Identification of the endosomal sorting complex required for transport-I (ESCRT-I) as an important modulator of anti-miR uptake by cancer cells. *Nucleic Acids Res.* 43, 1204–1215. <https://doi.org/10.1093/nar/gku1367>.

Wegner, C.S., Malerod, L., Pedersen, N.M., Progida, C., Bakke, O., Stenmark, H., and Brech, A. (2010). Ultrastructural characterization of giant endosomes induced by GTPase-deficient Rab5. *Histochem. Cell Biol.* 133, 41–55. <https://doi.org/10.1007/s00418-009-0643-8>.

Xu, B., Zhang, Y., Du, X.F., Li, J., Zi, H.X., Bu, J.W., Yan, Y., Han, H., and Du, J.L. (2017). Neurons secrete miR-132-containing exosomes to regulate brain vascular integrity. *Cell Res.* 27, 882–897. <https://doi.org/10.1038/cr.2017.62>.

## STAR★METHODS

## KEY RESOURCES TABLE

REAGENT or RESOURCE	SOURCE	IDENTIFIER
<b>Antibodies</b>		
Rabbit polyclonal anti-VPS28	Proteintech	Cat#15478-1-AP; RRID: AB_2878144
Rabbit polyclonal anti-Calnexin	Proteintech	Cat#10427-2-AP; RRID: AB_2069033
Rabbit polyclonal anti-TSG101	Proteintech	Cat#28283-1-AP; RRID: AB_2881104
Rabbit polyclonal anti-CD63	Proteintech	Cat#25682-1-AP; RRID: AB_2783831
Mouse Monoclonal anti-TUBB3	Proteintech	Cat#66375-1-Ig; RRID: AB_2814998
Rabbit polyclonal anti-HGS	Proteintech	Cat#10390-1-AP; RRID: AB_2118914
Mouse Monoclonal anti-Beta Actin	Proteintech	Cat#66009-1-Ig; RRID: AB_2687938
Mouse Monoclonal anti-VEGF	Santa cruz	Cat#sc-7269; RRID: AB_628430
Rabbit Monoclonal anti-VEGF	Abcam	Cat# ab52917, RRID:AB_883427
CoraLite488-conjugated Affinipure Goat Anti-Rabbit IgG(H+L) secondary antibodies	Proteintech	Cat#SA00013-2; AB_2797132
CoraLite594 – conjugated Goat Anti-Mouse IgG(H+L)	Proteintech	Cat# SA00013-3, RRID:AB_2797133
HRP-conjugated Affinipure Goat Anti-Mouse IgG(H+L)	Proteintech	Cat# SA00001-1, RRID:AB_2722565
HRP-conjugated Affinipure Goat Anti-Rabbit IgG(H+L)	Proteintech	Cat# SA00001-2, RRID:AB_2722564
<b>Chemicals, peptides, and recombinant proteins</b>		
VEGF121	GenScript	Accession # P15692-9
<b>Critical commercial assays</b>		
mMESSAGE mMACHINE T7 Kit	Invitrogen	Cat# AM1344
MAXIscript <i>In Vitro</i> Transcription Kit	Invitrogen	Cat# AM1314
Direct-ZoTM RNA MiniPrep	Zymo Research	Cat#R2052
HiScript II Q Select RT SuperMix	Vazyme	Cat#R233-01
PowerUp SYBR Green Master Mix	Thermo Fisher	Cat# A25742
ABclonal MultiF Seamless Assembly Mix	ABclonal Technology	Cat# RK21020
2X MultiF Seamless Assembly Mix	ABclonal Technology	Cat# RK21020
DAPI	Beyotime	Cat# C1002
<b>Protease</b>		
Trypsin-EDTA (0.05%)	Gibco	Cat#25300054
Fetal Bovine Serum	Gibco	Cat# 10099141
Poly-D-Lysine	Gibco	Cat#A3890401
Ham's F-12K	Gibco	Cat# 21127030
DMEM	Gibco	Cat# 11965084
Antibiotic-Antimycotic	Gibco	Cat# 15240062
Lipofectamine 3000	Invitrogen	Cat#L3000015
Opti-MEM	Gibco	Cat#31985088
Fetal Bovine Serum	SBI	Cat#EXO-FBS-50A-1
Collagenase D	Roche	Cat#11088858001
RIPA	Beyotime	Cat# P0013B
<b>Experimental models: Cell lines</b>		
Human: 293T cell	ATCC	CRL-3216
Mouse: primary neuron cell	This paper	N/A

(Continued on next page)

**Continued**

REAGENT or RESOURCE	SOURCE	IDENTIFIER
<i>Experimental models: Organisms/strains</i>		
Tg (kdr1: EGFP)	China Zebrafish Resource Center (CZRC)	ZFIN ID: ZDB-ALT-050916-14
Tg (Gata1: DsRed)	China Zebrafish Resource Center (CZRC)	ZFIN ID: ZDB-ALT-051223-6
Tg (vps28: eGFP)	This paper	N/A
vps28 <sup>+/-</sup>	This paper	N/A
Tg (huc: eGFP)	China Zebrafish Resource Center (CZRC)	ZFIN ID: ZDB-ALT-060301-2
Tg (kdr1: mCherry)	China Zebrafish Resource Center (CZRC)	ZFIN ID: ZDB-ALT-111104-1
<i>Oligonucleotides</i>		
siRNA targeting sequence: VPS28 #1 GAAGUGAAGUUGUACAAGATT	<a href="#">Wagenaar et al., 2015</a>	N/A
siRNA targeting sequence: VPS28 #2 AAUCAGCUCUAUUGACGAATT	<a href="#">Wagenaar et al., 2015</a>	N/A
Morpholino: MO-vegfaa GTATCAAATAAACCAAGTTCAT	Gene Tools	ZFIN ID: ZDB-MRPHLNO-050513-12
Morpholino: MO-tnt2a CATGTTTGCTCTGATCTGACACGCA	Gene Tools	ZFIN ID: ZDB-MRPHLNO-060317-4
SgRNA targeting sequence: vps28#1 GGACCGACCGATCACCATTAAGG	This paper	N/A
Primers for vps28, see <a href="#">Table S1</a>	This paper	N/A
Primers for this study, see <a href="#">Table S1</a>	This paper	N/A
<i>Recombinant DNA</i>		
pYSY-gRNA	YSY Biotech	N/A
Tol2-vps28-GFP	This paper	N/A
HuC:CD63-mCherry	This paper	N/A
huc: vps28	This paper	N/A
HuC:CD63-GFP	<a href="#">Xu et al., 2017</a>	N/A
Rab5CA (Q79L)-GFP	<a href="#">Bohdanowicz et al., 2012</a>	Addgene-35140
<i>Software and algorithms</i>		
Graphpad Prism	Graphpad Software	<a href="https://www.graphpad.com">https://www.graphpad.com</a>

**RESOURCE AVAILABILITY**

**Lead contact**

Further information and requests for resources and reagents should be directed to and will be fulfilled by the lead contact, Xiaohua Dong ([njfishxiaohua@163.com](mailto:njfishxiaohua@163.com)).

**Materials availability**

All plasmids or zebrafish lines generated in this study are available from the Lead Contact with a completed Materials Transfer Agreement.

**Data and code availability**

- All data reported in this paper will be shared by the lead contact upon request.
- This paper does not report original code.

- Any additional information required to reanalyze the data reported in this paper is available from the lead contact upon request.

## EXPERIMENTAL MODEL AND SUBJECT DETAILS

### Zebrafish

Zebrafish were raised under the standard conditions at 28°C in the zebrafish facility of the Model Animal Research Center, Nanjing University, and Tongren Hospital, Shanghai Jiao Tong University School of Medicine. The breeding and experimental protocols involved in using zebrafish were approved by the IACUC of the Model Animal Research Center, Nanjing University. The developmental stage of zebrafish was determined according to the previously reported (Kimmel et al., 1995). The following transgenic fish: *Tg (Kdrl: eGFP)*, *Tg (Huc: eGFP)*, *Tg (Gata1: DsRed)*, provided by the China zebrafish resource center were used in this study. The *vps28<sup>-22bp/+</sup>* mutant fish line and *Tg (vps28: eGFP)* transgenic line were generated in this study. 1-cell stage embryos or 30hpf stage larval were used for microinjection. Embryos used in this study were less than 3 dpf, which sex cannot be determined and unlikely to affect the results. The animal used in this study was approved by the Animal Ethics Committee of Tongren Hospital in China.

### Mouse primary cortical neuron culture and 293 T cell culture

Mouse primary cortical neurons were separated from postnatal 0 day C57BL/6 mouse. In brief, cerebral cortices were dissected and digested with 1 mL 0.25% trypsin at 37°C for 15 min and then replace trypsin with 10% F12/10% FBS in DMEM for stop digestion for two times. Dissociated cells then plated onto petri dishes coated with 0.01 mg/mL Poly-D-Lysine (Gibco) with 10% F12/10% FBS in DMEM for 4 h. After that, neurons were cultured in serum-free medium with 2% B27/1% Glutamax in Neurobasal medium in cell incubator at 37°C with 5% CO<sub>2</sub> and half medium were replaced every 3 days. And the replaced medium was collected for future EVs extracted. The sex of mouse used for primary cortical neuron culture was random.

HEK293T cell line was purchased from ATCC, and cultured in DMEM medium (Gibco, Grand Island, NY, USA) containing 10% fetal bovine serum (FBS, Gibco) and 1% penicillin-streptomycin (Gibco) in cell incubator at 37°C with 5% CO<sub>2</sub>. The sex of HEK293T cell came from is uncertain, but it is unlikely to affect the results.

## METHODS DETAILS

### Mutation and transgenic lines

CRISPR/Cas9 technology was used for generation of *vps28* mutants (Dong et al., 2014). Capped Cas9 mRNA were synthesized *in vitro* by using the mMACHINE T7 Kit (Ambion) (Dong et al., 2017). SgRNA were prepared to recognize the coding sequence of the exon 6 of *vps28*, and the target site of sgRNA was shown in Table S1. The templates of sgRNA were amplified by PCR with pYSY-gRNA vector (YSY, China) (Dong et al., 2017). sgRNA were synthesized using the MAXIscript *In Vitro* Transcription Kit (Ambion, USA). Cas9 mRNA and sgRNA were mixed and microinjected to 1-cell stage zebrafish embryos with a final concentration of 300 ng/μL:100 ng/μL. Founder (F0) were raised into adulthood and then crossed with wildtype to obtain next generation (F1). Then, when F1 was grown up, the genotype of F1 was identified by tail fin genomic PCR and sequencing to screening *vps28<sup>+/-</sup>* zebrafish (F1). *vps28<sup>+/-</sup>* were in-crossed to generate *vps28<sup>-/-</sup>* mutant embryos (F2) and used for the experimental analyses. Genotyping was used to identified between *vps28<sup>+/+</sup>*, *vps28<sup>+/-</sup>* and *vps28<sup>-/-</sup>*. Primers used for genotyping *vps28* mutants was shown in Table S1. Fragment sizes are 159 bp for *vps28<sup>+/+</sup>* and 137 bp for the *vps28<sup>-/-</sup>*, which could be identified by 2.5% agarose gel electrophoresis under 100 voltages for 30 min.

The *Tg (Vps28: GFP)* line was generated using the Tol2 transposon system. Zebrafish *Vps28* promoter fragment (1672 bp upstream of *vps28* translation start site) and GFP fragment were subcloned into the Tol2 vector. Primers used for generating the construct are given the Table S1. The recombined Tol2 plasmid (100 ng/μL) and transposase mRNA (300 ng/μL) were microinjected into 1-cell stage embryos to generation the founder (F1) of *Tg (Vps28: GFP)* line. The transgenic line was isolated by the expression of GFP in the next generation. *Tg (Vps28: GFP; Kdrl: mCherry)* fish were created by crossing individual transgenic line with the corresponding transgenic complement.

### Flow cytometry, RNA extracted, real-time PCR and whole mount *in situ* hybridizations

*Tg* (*Kdrl*: eGFP) and *Tg* (*Huc*: eGFP) embryos were used for EC and neuron sorting, respectively. Firstly, zebrafish embryos at 48 hpf were dechorionated with 0.5 mg/mL pronase (Roche, Switzerland) and washed with 1 × PBS for three times. Then the embryos were transferred into 15 mL tube containing 10 mL 0.25% trypsin (Gibco, California, USA) and were aspirated with the tips every 20 min for 2 h. Digested cells were collected by centrifugation with 200 g for 10 min at 4°C, suspended with 2% FBS/PBS solution, and then filtered with 40 μm cell strainer (BD Falcon, 352340). Finally, the cell suspension was used to sort out ECs or neurons by BD FACS Fortessa with 488 and 560 nm lasers.

Total RNAs of single zebrafish embryos, flow cytometry-sorted zebrafish ECs and neurons were extracted by using Direct-Zol™ RNA MiniPrep (Zymo Research, R2052, USA). Complementary DNA (cDNA) was synthesized with the HiScript II Q Select RT SuperMix for qPCR (Vazyme, R233-01, China). qPCR was performed by using PowerUp SYBR Green Master Mix (Thermo Fisher, A25742, USA) with ABI StepOne Plus. Whole mount *in situ* hybridization were performed as standard procedure (Dong et al., 2017). The primer sequences of specific genes are listed in Table S1.

### Transfection with siRNAs and plasmids in 293T cell

For knock down of VPS28 in 293T cell, two reported VPS28 siRNA were used in this study (Wagenaar et al., 2015). The sequence of siRNA were listed in key resources table. siRNA1 and siRNA2 were co-transfected into 293T cell with a final concentration of 10 nM.

Transfection were performed in a 6- well cell culture plate using Lipofectamine 3000 (Invitrogen, life technologies). Briefly, 5 μL of lipofectamine 3000 was mixed with 245 μL OpitiMEM (Gibco), 1.5 μL of siRNA1(20 μM) and 1.5 μL of siRNA2 (20 μM) or 3 μL negative control (20 μM) were mixed with 247 μL OpitiMEM (Gibco). siRNA mixture added into lipofectamine 3000 mixture and incubated for 5 min, the entire 500 μL mixture was added to a single well of 6- well cell culture plate. As for plasmids transfections, 2500 ng Rab5CA (Q79L)-GFP(Bohdanowicz et al., 2012) (Addgene plasmid 35140) or 2500 ng pCMV-CD63-mCherry plus 5 μL P3000 (Invitrogen, life technologies) and siRNAs were mixed with OpitiMEM (Gibco), plasmids/P3000/siRNA/lipofectamine 3000 mixture incubated for 5 min and then added to a single well of 6-well cell culture plate. At 24 h post-transfection, the cells were changed with fresh media and prepared for immunofluorescence or imaging after 48 h post-transfection.

### EVs collection from *in vitro* cultured 293T cell, primary cortical neuron and zebrafish embryos

293T cell was cultured in DMEM supplemented with 1% penicillin-streptomycin and 10% EVs-depleted FBS (EXO-FBS-50A-1, SBI, USA). Cell culture supernatant were collected at 24, 48 and 72 h after transfected with VPS28 siRNA. The supernatant of primary cortical neuron was collected every 3 days during the cell culture. The supernatant of zebrafish embryos was obtained as follow step, about 150 zebrafish embryos of 54 hpf were treated with Collagenase D (Roche), used at a concentration of 2 mg/mL in a total volume of 1.5 mL. Embryos were incubated at 37°C for 30 min, while the sample was intermittently crushed through 1 mL syringes to make the large clumps disappeared.

Then, the EVs from 293T cell, primary cortical neuron and zebrafish embryos were collected by serial centrifugation as follows. 320 g for 10 min, 2000 g for 15 min at 4°C (precipitates were collected as 2k pellet), 10,000 g for 30 min, and ultracentrifugation at 100,000 g for 70 min at 4°C. EVs pellet were washed in cooled PBS and obtained by ultracentrifugation at 100,000 g for 70 min at 4°C (Optima XPN-100 Ultracentrifuge, Beckman Coulter).

### Microinjection of plasmid, morpholino, EVs, VEGF-A and DAPI into zebrafish embryos

HuC:CD63-GFP plasmid kindly provide by Prof. Jiulin Du lab(Xu et al., 2017). HuC:CD63-GFP (75 ng/μL) plasmid is microinjected into 1-cell stage embryos to detected the expression of GFP in *vps28* mutants. For rescue assay, HuC: *vps28* (50 ng/μL) plasmid is microinjected into 1-cell stage embryos. *vegfaa* and *tnnt2a* antisense oligonucleotides are designed as previously described and obtained from Gene Tools (Jin et al., 2017; Nasevicius et al., 2000). The sequence of *vegfaa* MO and *tnnt2a* MO are listed in key resources table. 8 ng of *vegfaa* MO and 4 ng of *tnnt2a* MO is microinjected into 1-cell stage of zebrafish embryos to generate the specific morphants. EVs (10<sup>9</sup> particles/μL) derived from wildtype embryos and *vegfaa* morphants at 54hpf is microinjected into the 1-cell stage embryos.

VEGF-A protein, primary neuron cell derived-EVs and wildtype embryos derived- EVs microinjected into the blood circulation system through the common cardinal vein (CCV) at 30hpf, respectively. 10 mg/mL DAPI (Beyotime, China) was injected into the blood circulation system at 54 hpf and taken confocal images immediately after injection.

### Plasmid construction

pCMV5 were digested with EcoRI and XbaI, CD63 and mCherry were cloned into pCMV5 with primers listed in Table S1 by ABclonal MultiF Seamless Assembly Mix (RK21020, ABclonal Technology, Wuhan, China). For huc:vps28 construct, the HuC promoter sequences was subcloned from HuC:CD63-GFP with primer listed in Table S1, the vps28 CDS fragment was obtained with the primer listed in Table S1, and then the huc containing fragment, vps28 containing fragment and pGEM-T easy vector fragment were mixed with 2X MultiF Seamless Assembly Mix followed their operation manual (RK21020, ABclonal Technology, Wuhan, China).

### Immunofluorescence

For immunofluorescence assays, cells were plated onto slides (YA0352, Solarbio, Beijing, China), cultured for 12 h, fixed with 4% paraformaldehyde for 20 min at 4°C. Cells were incubated for HGS Rabbit Polyclonal antibody (Proteintech, 10390-1-AP) (1:100), Mouse Monoclonal anti-TUBB3 (Proteintech, 66375-1-Ig), VPS28 antibody (Proteintech, 15478-1-AP) and Anti-VEGFA antibody [EP1176Y]-C-terminal (Abcam, Cat#ab52917), followed by CoraLite488-conjugated Affinipure Goat Anti-Rabbit IgG(H+L) secondary antibodies (Proteintech, SA00013-2) (1:250) or CoraLite594 – conjugated Goat Anti-Mouse IgG(H+L) (Proteintech, SA00013-3), respectively. Cells were transfected with Rab5CA (Q79L)-GFP and pCMV-CD63-mCherry, fixed with 4% paraformaldehyde. Samples were examined with ZEISS LSM880 confocal microscope (Zeiss) and images were processed using ZEN software.

### Western blot

Cells, cell pellet and EVs pellet were lysed with RIPA (Radio Immunoprecipitation Assay) lysis buffer (P0013B, Beyotime, Shanghai, China) containing 1 mM PMSF (Phenylmethanesulfonyl fluoride) (ST506, Beyotime, Shanghai, China). Proteins were separated by 8%–20% acrylamide/bisacrylamide gels and transferred to PVDF membranes (Millipore, Billerica, USA). The proteins were blocked in 5% blocking reagent (1×TBST containing 5% defatted milk powder) for 1 h at room temperature. Membranes were incubated with primary antibodies (1:1000–1:3000) in antibody dilution buffer (G2025, Servicebio, Wuhan, China) for overnight at 4°C. After that, membranes were washed with 1×TBST for three time and then incubated with HRP (horseradish peroxidase)-conjugated second antibodies (1:1000–1:5000) in antibody dilution buffer for 1 h at room temperature. The proteins were visualized with Tanon 6200 (Tanon, Shanghai, China). The following antibodies were used, rabbit anti-human VPS28 (Proteintech, 15478-1-AP), rabbit anti-human Calnexin (Proteintech, 10427-2-AP), rabbit anti-human TSG101 (Proteintech, 28283-1-AP), rabbit anti-human CD63 (Proteintech, 25682-1-AP), anti-human  $\beta$ -Actin (Proteintech, 66009-1-Ig) and anti-mouse VEGF (Santa cruz, sc-7269).

### NTA measurement

EVs particle size and concentration were measured by NTA at Viva Cell Biosciences with ZetaView PMX 110 (Particle Metrix, Meerbusch, Germany) and corresponding software ZetaView 8.04.02. Isolated total EVs samples were diluted to 100  $\mu$ L 1X PBS buffer. Concentrated samples were pre-diluted 300x, and were measured at 11 different positions with stage temperature control set at 27°C.

### Confocal imaging

Larvae were embedded in 1% low-melting agarose (BBI Life Sciences, Shanghai, China) at 54 hpf at room temperature. Time-lapse images were taken with a 10-min interval, Z-stake of imaging ranged from 10 to 15  $\mu$ m with the interval 2  $\mu$ m. Imaging was captured with Zeiss LSM880 confocal microscopy (Zeiss, Germany).

### Transmission electron microscopy

A total 10  $\mu$ L isolated EVs were put on a formvar/carbon-coated copper grid for 10 min and were fixed in 1% glutaraldehyde for 10 min, washed in water, and contrasted in a uranylacetate/methylcellulose mix for

10 min at room temperature to negatively stain the exosomal fractions. Then the samples were examined immediately at 80 kV with a JEM-1011 transmission electron microscope.

Larvae at 2 dpf were fixed in 2.5% glutaraldehyde overnight at 4°C. Preparations were then washed with 0.1 M phosphate buffer (pH = 7.4) for three times with 15 min interval. Dehydrated through a graded with acetone series, and embedded in Epon812 (PELCO, 18010). Ultrathin sections (70 nm thickness) were prepared, stained with uranyl acetate (PELCO, 19481) and lead citrate (TEDPELLA, 19312), and examined by electron microscopy (Tecnai G2 Spirit Biotwin).

#### **QUANTIFICATION AND STATISTICAL ANALYSIS**

Data were analyzed by Graphpad Prism (Version 9.0.0) using t tests between two groups. Differences were considered significant with  $p < 0.05$ . Error bars indicate SD.